Prospects for accelerated development of high performance structural materials

Steven J. Zinkle [a,*], Nasr M. Ghoniem [b]

[a] Oak Ridge National Laboratory, P.O. Box 2008, Oak Ridge, TN 37831, USA
[b] University of California at Los Angeles, Los Angeles, CA 90095, USA

ARTICLE INFO

ABSTRACT

We present an overview of key aspects for development of steels for fission and fusion energy applications, by linking material fabrication to thermo-mechanical properties through a physical understanding of microstructure evolution. Numerous design constraints (e.g. reduced activation, low ductile–brittle transition temperature, low neutron-induced swelling, good creep resistance, and weldability) need to be considered, which in turn can be controlled through material composition and processing techniques. Recent progress in the development of high-performance steels for fossil and fusion energy systems is summarized, along with progress in multiscale modeling of mechanical behavior in metals. Prospects for future design of optimum structural steels in nuclear applications by utilization of the hierarchy of multiscale experimental and computational strategies are briefly described.

© 2011 Elsevier B.V. All rights reserved.

1. Introduction

The demanding service environment associated with proposed fusion energy systems will require a wide range of materials that are tailored for high performance in a hostile environment involving intense heat fluxes, high temperatures, potentially corrosive coolants, significant cyclic thermomechanical stresses, and intense fluxes of high-energy neutrons and electromagnetic radiation. The technological challenges associated with development of structural materials for fusion energy have been summarized by numerous authors [1–11].

Significant progress has been achieved in the operational performance and radiation resistance of structural materials during the past few decades. For example, original research on structural ceramics based on monolithic materials has rapidly progressed through a series of increasingly high-performance and radiation-resistant ceramic fiber reinforced ceramic matrix composites [12–14]. Similarly, steels such as HT-9 originally developed in the 1960s have evolved into high-performance 9%Cr reduced-activation ferritic–martensitic steels with superior mechanical performance in unirradiated and irradiated conditions [15–18]. Very high performance oxide dispersion strengthened (ODS) steels are being investigated in worldwide research programs for potential transformational mechanical properties and radiation-resistance [19–23]. Such progress was achieved through a combination of experimentation, modeling and empirical information. Further development and optimization of structural steels in nuclear applications will require full utilization of an array of sophisticated experimental techniques and multiscale computational modeling, in addition to empirical data.

2. Constraints on the development of structural materials for fusion energy

Development of structural materials for fusion energy is guided by the operational conditions expected in fusion power plants, and by lifetime and safety requirements associated with economics and environmental concerns. The operational conditions necessitate the use of structural materials at high temperatures in order to achieve high thermodynamic efficiency, as well as at low temperatures dictated by normal shutdown and start-up operations along with maintenance of plant components. In the following, we discuss the key physical phenomena that lead to constraints imposed by the neutron radiation environment, followed by a brief discussion of anticipated mechanical failure modes.

2.1. Key radiation damage phenomena

Exposure to energetic neutron irradiation can create numerous changes in materials. The five key phenomena of highest significance for establishing viable operating temperatures and doses of structural materials are [11,24]: Low temperature radiation hardening and embrittlement, which typically emerges for displacement damage levels above 0.001–0.1 displacements per atom (dpa) at temperatures below $\sim 0.4 T_M$, where T_M is the melting temperature; potential matrix and/or grain boundary embrittlement due to radiation-enhanced or –induced precipitation due to coupled solute–defect processes that are typically most prevalent at doses above 1–10 dpa at intermediate temperatures of $0.3–0.6 T_M$;

* Corresponding author. Tel.: +1 865 576 5785; fax: +1 865 241 7603.
E-mail address: zinklesj@ornl.gov (S.J. Zinkle).

plastic deformation due to irradiation creep (acting in addition to thermal creep processes) that is most significant for doses above 10 dpa at irradiation temperatures below $0.45T_M$; volumetric swelling due to void formation that is typically of concern for damage levels >10 dpa at intermediate temperatures of $0.3–0.6T_M$; and high temperature helium embrittlement of grain boundaries, which typically is a major issue in mechanically stressed materials for transmutant helium concentration levels above ~10–100 appm (>1–10 dpa) at exposure temperatures above $0.5T_M$. In most structural materials, the first and last of these five phenomena define the lower and upper bounds for viable operating temperatures, and the other three listed phenomena typically determine the maximum viable operating lifetime. The key challenges for developing improved radiation-resistant structural materials are centered on two major topics: expanding the viable operating temperature window, and expanding the viable operational lifetime of structural materials.

2.2. Mechanical failure modes

Mechanical failure of structural materials due to static or cyclic stress in an irradiation environment is a primary feasibility issue. Mechanical deformation and fracture modes [25–29] can be prompt (at or near the start of operations), or delayed (property degradation from cumulative damage due to thermal, stress, corrosion and radiation effects):

- Monotonic stress-induced failure (e.g., Refs. [4,30–35]), which includes (a) prompt plastic collapse, (b) prompt plastic instability due to large deformation or flow localization, (c) prompt fracture (brittle or with exhaustion of ductility), and (d) thermal creep cavitation and rupture.
- Cyclic stress-induced failure (e.g., Refs. [4,32,35–37]), including (a) progressive deformation (ratcheting), (b) progressive cracking (fatigue), and (c) fatigue-creep type failure.
- Irradiation-accelerated and -induced failure (e.g., Refs. [27, 32,34,36,38–40]), including (a) prompt irradiation-induced plastic instability due to flow localization, (b) irradiation-induced prompt fracture due to hardening, loss of ductility, and embrittlement due to defect clusters, helium and phase instabilities, (c) irradiation-accelerated thermal creep cavitation and rupture, including helium embrittlement [41], and (d) dimensional instabilities due to irradiation creep and swelling [42–44].

Although not covered here, it should be noted that section thinning due to corrosion (either uniform or localized) and stress-assisted corrosion cracking are often the dominant lifetime engineering issues facing power conversion systems (because major stress-induced failure issues have been accommodated by material selection and utilization of conservative engineering design rules). There are numerous material-coolant and material–material compatibility issues not discussed in this paper that need to be considered for determination of viable operating temperatures [45].

As an example of failure mode considerations, Fig. 1 shows the operational window of the first wall/blanket component in an early fusion power plant conceptual design, where ferritic/martensitic steels were first considered [46]. Those initial simplified analyses suggested the design window of ferritic/martensitic steels would be dictated by radiation-induced embrittlement at temperatures below 350 °C, and by thermal creep rupture at temperatures above 550 °C. It is to be noted this design window was based on simplifying assumptions and did not consider all the failure modes discussed above. More detailed design and analysis will be required for qualification of structural materials as fusion energy research moves toward power production [4,18,27,47,48]. In addition to

mechanical stress and radiation effects issues, other engineering issues including corrosion, stress concentrators and/or nonuniform properties due to joining will need to be evaluated.

3. Key concepts for development of ferritic/martensitic (F/M) steels

3.1. Development of steels for non-fusion applications

The development of structural steels for fusion applications is closely linked to the larger worldwide efforts on development of high-temperature steels for fossil energy and chemical processing applications. The general methodology for optimization of steel properties has utilized extensive semi-empirical correlations between material processing techniques, the resultant microstructure, and the mechanical properties. Several generations of high-temperature steels with successively improved high temperature strength have been developed [11,16,49,50]. Viswanathan [50] categorized the development of modern steels into several generations based on successive improvements of their long-term creep strength. First generation steels developed during the 1960s (e.g., HT-9 and EM-12) introduced carbide-forming elements such as V, Nb and W. Second generation steels (1970–1985) such as T-91 refined the C, N, V and Nb concentrations to produce more finely dispersed precipitates. Third generation (1985–1995) steels such as T-92 or NF-616 introduced W, Cu, N and B for improved strength. Using the metric of rupture stress (σ_R) at 600 °C for a time period of 10^5 h (11.4 years), the strength of steels has increased from 40 MPa for "zeroth" generation steels such as the initial 9%Cr–1%Mo (T9) steels that were developed in the 1950s to approximately 180 MPa in current (fourth generation) steels such as the 12%Cr steels NF-12 and SAVE-12 that contain optimized concentrations of C, Nb, Mo, V, W and Co. The corresponding maximum use temperature for steels has increased from 525 °C for zeroth generation steels to 650 °C for 4th generation steels [11,50], with a remarkably constant rate of improvement of 2.5 °C per year achieved over the past 55 years [11]. Table 1 summarizes the role of solute additions in current steels [49].

3.2. Development of steels for fusion energy

Development of ferritic/martensitic steels for fusion energy applications has followed a parallel path to the approach described above. However, a fundamental difference between steels for fusion energy and conventional applications is the importance of reduced activation (both short-term decay heat and volatilization issues and long-term radioactivity associated with fusion neutron-induced transmutation reactions) [51], which limits the number of acceptable solute elements to a small fraction of the periodic table. In addition, the intense neutron radiation environment and high levels of transmutant helium require fusion reactor steels to be designed with high radiation resistance. Both fusion and fossil energy applications require steels with highly stable precipitates (along with matrix solution hardening elements). For fossil applications, the precipitates need to resist coarsening or dissolution at elevated temperatures for lifetimes that may exceed 40 years (compared to an anticipated ~5–10 years lifetime for replaceable fusion energy structures) The shorter required lifetime for fusion energy steels is offset by the extremely demanding irradiation environment that may induce precipitate coarsening or dissolution that would not occur in a non-irradiation environment.

In order to minimize δ-ferrite and radiation-induced α' phases, which reduce fracture toughness, steels with 7–9%Cr are preferred compared to higher chromium alloys [16,52]. Fig. 2 summarizes the superior ductile to brittle transition temperature (DBTT)
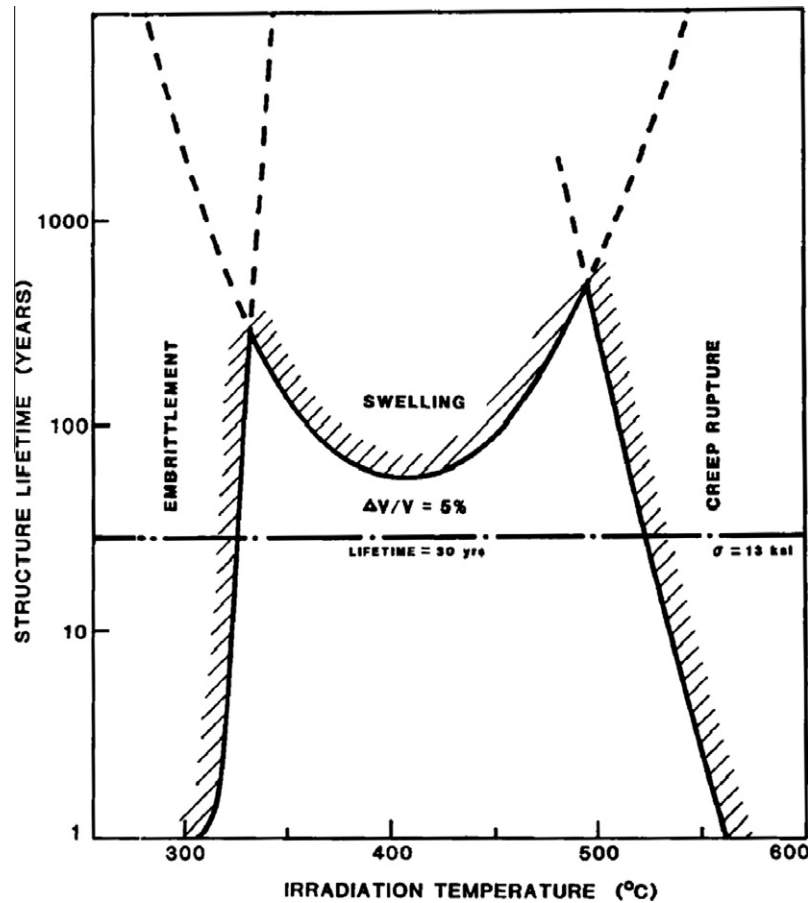
Fig. 1. Operational design window for the FW/B of a conceptual fusion power plant (magnetic mirror design), where early versions of ferritic/martensitic steels were proposed [46].

Table 1
Relationship between composition and microstructure of ferritic/martensitic steels [49].

Element	Microstructure function
C, N	Austenite stabilizers, low solubility in ferrite, form carbides, nitrides and carbonitrides
Cr	Corrosion resistance, ferrite stabilizer, forms $M_{23}C_6$ (high Cr steels) and M_7C_3 (low Cr steels)
Mo, W	Ferrite stabilizers, form stable carbides, limited concentration to avoid δ-ferrite, distributed between M23C6 and solid solution, (Mo + 0.5 W) < 1.5% to avoid laves phase removing them from solution
V, Ta, Nb	Form M(C, N) stable carbides, restrict grain growth during austenitization
B, P	Surface active elements, segregate to grain boundaries, increase hardenability, slow down $M_{23}C_6$ coarsening, 0.005–.01%
Ni, Mn, Co	Austenite stabilizers, increase toughness, prevent δ-ferrite during austenitization and result in 100% martensite phase
Cu	Austenite stabilizer, low solubility in ferrite, precipitates during normalization and ageing, may increase creep strength

behavior for neutron irradiated 7–9%Cr steels compared to 12%Cr and 17%Cr steels [53,54]. From safety considerations, it is desirable for the structural components to retain high toughness during operation at elevated temperatures as well as at lower temperatures that might occur during shutdown for maintenance procedures. In Fig. 2, the DBTT of 9%Cr steels remains below room temperature for irradiation temperatures >375 °C. For 12%Cr steels, the DBTT falls below room temperature only for irradiation temperatures above 450 °C, and for 17%Cr steels the DBTT remains above room temperature for all irradiation temperatures.

Initial [55] and subsequent [15,17,56–60] alloying modifications to incorporate reduced activation considerations for fusion energy steels have led to the elimination of Mo, Nb, Ni, Co, Cu and N, and the introduction of W and V as carbide formers in place of Mo, while Ta was introduced as a replacement for Nb. Due to their good combination of corrosion and radiation embrittlement

resistance, international research [7,60] has recently focused on 8–9%Cr steels with composition range (wt%): Cr 8–9, W 1–2, Mn ∼ 0.45, V ∼ 0.2, Si 0.05–0.3, Ta 0.04–0.1, C ∼ 0.1, N 0.01–0.05, B < 0.003) and include alloys such as F82H, JLF-1, EUROFER and EUROFER-97 [61].

4. Progress in the development of high-temperature steels

There are two general approaches for the science-based development of new high-performance steels, both of which require utilization of state of the art modeling and simulation in close connection with experimental validation studies. In the first (evolutionary) approach, alloy fabrication is based on classical ingot metallurgy techniques and high strength is designed on the basis of well-established solid solution strengthening and
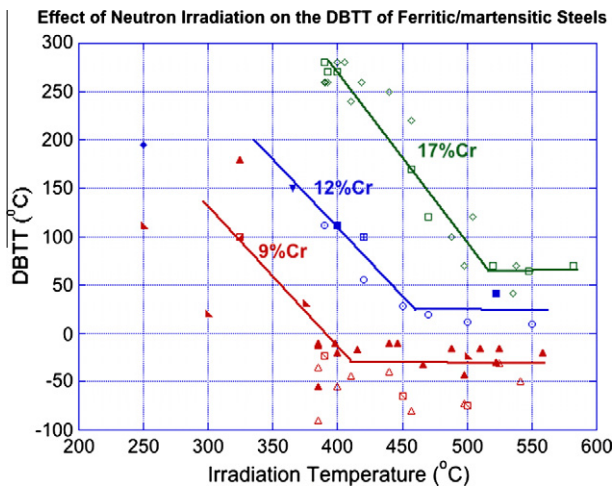
Fig. 2. Effect of neutron irradiation on the ductile to brittle transition temperature in 9–17% ferritic/martensitic steels based on data summarized in Refs. [53,54].

precipitation hardening principles. Semi-empirical processing–structure–property relationships are often used to rapidly converge on a desired composition, thermomechanical processing schedule, and microstructure that will produce improved performance. Computational thermodynamics and complementary multiscale computer modeling analyses such as *ab initio* energy evaluations or Molecular Dynamics simulations of precipitate hardening barrier strengths are typically utilized to guide the design of new alloys. This "material by design" approach [62] has successfully led to the rapid discovery of numerous new high performance structural materials for non-fusion applications. The second general approach, which is beyond the scope of the present paper, is based on nonconventional processing techniques (e.g., powder metallurgy, friction stir processing, engineered micro- or nano-laminate architectures, near-net-shape direct manufacturing, etc.) which may lead to novel microstructures and material properties that could not be achieved by conventional alloy processing techniques.

The extraordinary value of computational thermodynamics to rapidly search through a wide range of compositional combinations can be clearly understood when one considers that modern steels typically consist of about 10 solutes added to the base iron composition. For example, the P92 (Fe–9%Cr–2%W) steel contains 12 solutes with specified allowable composition ranges, plus maximum composition limits for phosphorous and sulfur. Empirical exploration of the phase stability of such multi-composition steels would require fabrication of numerous independent heats to examine multiple compositions of each solute species. From elementary combinatorial probability principles, the number of combinations for an alloy consisting of 10 solutes with four compositional variations for each solute is 4^{10}, i.e., slightly more than one million choices. Therefore, it is not possible to experimentally investigate the phase stability for even a fraction of the possible solute combinations of a given steel. On the other hand, by employing automated iterative computational thermodynamic calculations, it is possible to explore on a workstation computer within a couple weeks the phase stability for up to one million compositional variations in a steel [63].

There are numerous recent examples of high-performance steel development where advanced microstructure-properties information (often in the form of computational modeling) played an integral role. In particular, many of the advances required innovative solutions to competing effects caused by the introduction of different solute atoms. For example, in the development of the CF8C-Plus

cast austenitic stainless steel, it was recognized that formation of stable nanoscale MC carbide dispersions for dislocation pinning and reduction of the grain boundary embrittling FeCr sigma phase could be achieved by enhancing (substituting) Nb compared to Ti and increasing the C and P content while decreasing the N content [64]. Similarly, development of high-strength alumina-forming austenitic stainless steels that would enable corrosion resistance in oxidizing environments at temperatures above 700 °C has been an elusive goal for the past 40 years. Recent work utilizing computational thermodynamics led to the discovery that high creep strength up to 800 °C and creation of an alumina self-healing surface oxide could be achieved by carefully balancing the amounts of Al, Nb, Hf, Y and Cr [65–67].

Similar success has been achieved in rapidly designing high-performance ferritic/martensitic steels for fossil energy ultrasupercritical steam systems and for fusion energy applications. In general, clear knowledge of the dominant deformation mechanisms [25,27] is important for designing improved strength; for example, adding matrix precipitates is not helpful if the creep deformation mechanism is due to boundary sliding/diffusional creep mechanisms. An analysis of the thermal creep deformation mechanisms for a 9%Cr–3%W ferritic/martensitic steel indicated deformation was dominated by diffusional creep along grain boundaries and sub-boundaries [68,69]. Introduction of nanometer-scale, thermally stable carbonitride precipitates along grain boundaries to pin their movement produced approximately two orders of magnitude improvement in thermal creep rupture lifetime at 650–700 °C. Utilization of new thermomechanical heat treatment conditions in combination with microalloying modifications has resulted in the creation of new steels with significantly improved strength without sacrificing ductility [70–74]. The thermal creep strength of a modified 9%Cr–1%Mo steel was doubled at 650 °C, and the corresponding thermal creep lifetime at 650 °C for an applied stress of 120–140 MPa was improved by about two orders of magnitude [71,73] due to the formation of a high density of nanoscale vandium- and niobium-rich MX precipitates associated with the controlled nitrogen additions and new thermomechanical treatment. Fig. 3 compares the thermal creep strength at 650 °C for thermomechanically-treated and conventionally-treated 9%Cr–1%Mo steels. The IEA fusion materials reduced activation steel F82H is also included in Fig. 3 for comparison.

Development of reduced activation ferritic/martensitic steels for fusion energy applications is at an intermediate level of maturity.
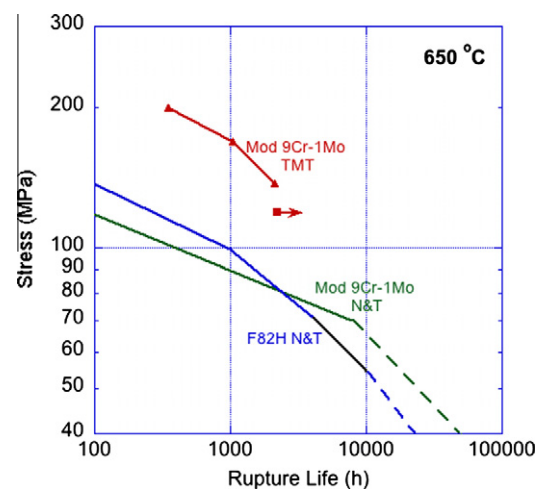

Fig. 3. Comparison of creep rupture behavior of 9%Cr Steels at 650 °C after conventional and new thermomechanical treatment [71,73].

The properties of the current IEA reference Fe–8–9%Cr–2%W fusion steel is comparable to the best Generation II [16,50] conventional steels. This reduced activation steel was developed using traditional steelmaking principles, without utilizing computational thermodynamics tools. Considering the advances that have been achieved from Generation II to Generation IV conventional steels, this suggests it may be possible to develop new grades of reduced activation steels with improved mechanical properties and potentially improved radiation resistance and/or tailored properties such as self-healing corrosion-resistant surface coatings or tritium permeation barriers. It would be valuable to continue to pursue the development of new reduced-activation steels using computational design tools in addition to classical steelmaking procedures.

Recent studies are also exploring the potential of new formulations of oxide dispersion strengthened (ODS) ferritic steels containing 8–14%Cr, which may enable much higher operating temperatures due to superior thermal creep strength compared to standard ferritic/martensitic steels [19–23] and may provide improved fracture toughness [75] (compared to earlier ODS steels) and superior radiation resistance to void swelling and high temperature helium embrittlement [22,76]. Microstructural and compositional variables being examined include the addition of Al to provide improved corrosion resistance to steam [77,78] and liquid metal [79] coolants, and utilization of nanoscale grain sizes to produce improved and more isotropic mechanical properties before and after low temperature neutron irradiation [75]. A wide variety of processing conditions and solute contents are currently being explored in an attempt to identify the optimized ODS reduced activation ferritic/martensitic steel for fusion applications [21,77,80,81]. However, to date only limited modeling and simulation has been used to guide the development of ODS steels. Key research challenges include identification of processing and compositional changes to increase the duration of the tertiary thermal creep regime, improving high temperature fracture toughness, examination of potential embrittlement in the 12–14%Cr alloys due to α' and other precipitation reactions, and identifying viable ODS steel joining mechanisms such as friction stir welding. Improved understanding of the atomistic composition of the nanoclusters and the effect of intense neutron irradiation on the cluster composition and stability is also needed.

5. The role of multiscale modeling in alloy design

Multiscale modeling offers significant potential advantages to accelerate the development of high-performance structural materials by enabling detailed simulation of mechanical properties, calibration with microstructure-based experimental data, and prediction of optimal properties based on microstructure [82,83]. In particular, improved models for dislocation–obstacle interactions that go beyond simplistic barrier strength correlations and more detailed models of point defect interactions with microstructural features can provide valuable insight for developing high performance radiation-resistant materials. Unfortunately, the current modeling connections between microscopic mechanisms of mechanical property changes and structural failure mechanisms at the different length and time scales are incomplete, and improved integration is needed. We briefly describe here a few examples of recent advances in multiscale modeling "building blocks" that are contributing to a deeper understanding of the relationship between the microstructure, strength and ductility.

5.1. Modeling the core structure and properties of dislocations in BCC metals

Experimental studies have demonstrated that solutes can give rise to both solid-solution hardening (SSH) and solid-solution softening (SSS) [84]. The dislocation behavior is often variable in commercial-purity alloys, where dislocation mobility can vary by several orders of magnitude. This significant influence induced by small amounts of solutes is of great practical importance to body centered cubic (BCC) metals, in particular refractory metals (Nb, W, Ta, and Mo). Continuum elasticity theory has provided considerable insight of SSS/SSH in terms of the size and elastic constants between the solute and host atoms. The correlation between the hardening rate and number of conduction electrons of transition-metal solutes, however, indicates a nonlinear *chemical* origin of the dislocation–solute interaction [85,86]. Recently, a first-principles Greens function boundary condition method study [87] confirmed that solid solution softening by transition-metal solutes in Mo is attributable to a large chemical effect on the dislocation core and hence the mobility of dislocations.

A multiscale approach that includes dislocation long-range elastic fields and solute-host atomic interactions in the core region has been recently developed [88]. In order to study the effect of local solute environment on the mobility of screw dislocations, dilute random solid solutions and small solute clusters were investigated in W–Ta alloys which are known to exhibit SSS or SSH under different test conditions [89]. The stresses necessary to induce dislocation motion on the (0 1 1) glide plane were observed to be strongly dependent on the solute distribution and precipitate geometry, producing either solute softening or hardening. In all cases, W solutes had a small effect on the polarization, indicating the W–Ta Peierls stress is not influenced by polarization.

Several multiscale methods have been developed to examine the dislocation core structure, properties and interactions in metals [90]. For non-magnetic BCC tantalum, theoretical studies have led to two types of core structures: asymmetric and symmetric [91]. The dislocation core structure of BCC Fe has an additional complication arising from the presence of magnetism, which cannot be accurately simulated with empirical interatomic potentials [92]. *Ab initio* calculations reveal the screw dislocation core is altered from non-polarized in pure Fe to a polarized structure when Cu nanoprecipitates are incorporated in the core. In contrast, Cr clusters do not change the core polarization and increase the Peierls stress, thus hardening Fe [90]. The hybrid *ab initio* approach of Suzuki's atomic-row (AR) model for a screw dislocation in BCC metals offers a plausible compromise between computational efficiency and accuracy. The inter-row potential (IRP), derived from *ab initio* calculations, allows the treatment of solutes in the core, while the dislocation core structure is determined by relaxing the ARs using the IRP, similar to atomistic simulations employing interatomic interactions. Total-energy calculations indicate that Cu solutes act as lubricants and facilitate the shear process between the Fe–Cu and Cu–Cu rows.

Several studies have observed transformation of Cu precipitates in iron from the BCC to the 9R faulted face centered cubic phase for diameters above $d \sim 5$ nm [93,94]. Atomistic simulations of the interaction between dislocations with Cu precipitates of sizes 1–6 nm indicate two different deformation mechanisms exist [95,96]. At small sizes near 2 nm, the precipitate is sheared and the dislocation core structure transforms from polarized to non-polarized upon exiting the precipitate. For Cu precipitates with $d > 4$ nm, Orowan looping occurs around the impenetrable precipitates.

5.2. Modeling the interaction between dislocations and precipitates

In order to model dislocation interaction with precipitates in 3-D, a computational method that combines Parametric Dislocation Dynamics (PDD) and the Boundary Element Method with volume integrals was recently developed [97]. The method allows calculations of the stress field both inside and outside precipitates with
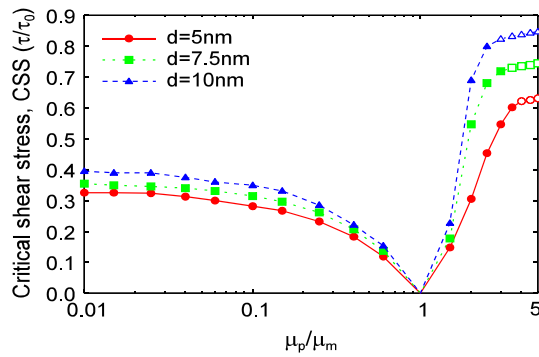
Fig. 4. Dependence of the critical shear stress on the precipitate-to-matrix shear modulus ratio. The effect of the precipitate diameter on the strength is shown, where the solid symbols are for dislocations cutting through precipitates while the hollow symbols are for the Orowan looping mechanism.

Fig. 5. Critical resolved shear stress for dislocations to bypass Y_2O_3 particles. The dashed line is an analytically calculated Orowan stress.

elastic moduli (μ_p) different from the matrix (μ_m), and that may have initial coherency strain fields. Simulation results for precipitate diameters of 5–10 nm are shown in Fig. 4, where the critical strength is normalized by the reference shear stress $\tau_0 = \mu_m b / L$. The precipitate strength increases with precipitate size and is dependent on the relative elastic modulus mismatch. Soft precipitates ($\mu_p/\mu_m \leqslant 1$) produce moderate strengthening, and in the limit of very soft precipitates (e.g. voids) the strengthening effect saturates to $\tau/\tau_0 \approx 0.3$–0.4. On the other hand, harder precipitates are still shearable up to μ_p/μ_m ratios on the order of 3–4, whereupon the Orowan looping mechanism sets in, as shown in the open symbols in Fig. 4. Sheared copper precipitates (2.5 nm in diameter) lose some of their resistance to dislocation motion after they are cut by dislocations in a pileup. Successive cutting of precipitates by dislocations reduces the barrier strength to about half its original value when the number of transmitted dislocations exceeds about 10 [97].

A recent modeling study investigated the dislocation core structure of Y_2O_3 oxide dispersion strengthened steels, on the basis of γ-surface energies [98]. The dislocation interaction with Y_2O_3 particles was simulated using a combination of 2-dimensional Dislocation Dynamics (DD) and generalized Peierls–Nabarro model, as well as 3-D PDD simulations [98]. Fig. 5 shows the dependence of the critical resolved shear stress (CRSS) on the vertical distance from the precipitate mid-plane (z). The estimated Orowan stress is also plotted, where μ is the elastic shear modulus of iron, b is the Burgers vector and L_0 is the spacing between Y_2O_3 particles on the dislocation slip plane. The simulation CRSS is 50–90% of the analytic Orowan stress, depending on the slip plane location. The simulation results indicate the CRSS is asymmetric with a maximum at $z/D = -0.2$, which differs from the symmetric Orowan estimate (maximum at $z/D = 0$). When the slip plane position z/D is negative, the dislocation has an initial attractive interaction with the Y_2O_3 particle (mainly due to lattice mismatch). However, at later stages of the dislocation bypass process, the interaction changes to a repulsive one, rendering it difficult to complete the Orowan looping. On the other hand, for positive z/D slip plane positions, the CRSS decreases rapidly since the interaction changes from repulsive to attractive at the later stages of the dislocation bypass process.

5.3. Modeling plasticity of irradiated materials

It is widely appreciated that plastic strain in metals is fundamentally heterogeneous, displaying high strains concentrated in small material volumes, with virtually undeformed regions in-between [99]. Irradiated steels exhibit such heterogeneous plastic
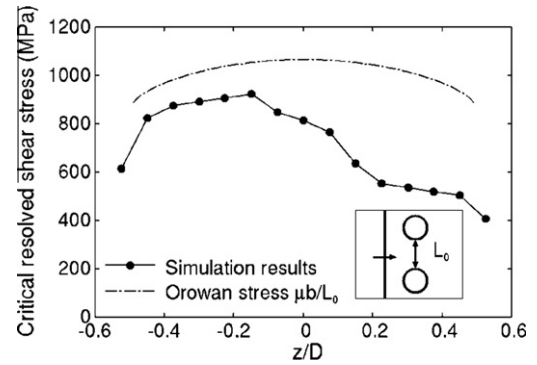
deformation via localized plastic flow (called dislocation channeling) [100,101]. The fundamental mechanisms of radiation hardening and dislocation channel formation due to dislocation destruction of point defect clusters have been studied by MD simulations [102–106], and confirmed by in situ experiments [107]. A recent alternative mechanism for loss of uniform elongation, based on a material-specific plastic instability stress criterion, has also been found to satisfactorily explain the observed behavior in many irradiated metals [108].

Two main approaches for modeling the mechanical behavior in the meso length scale [109] are based on statistical mechanics methods and Dislocation Dynamics [110,111]. Recent Dislocation Dynamics simulations [112] have examined the role of dislocation pileups on the creation of cleared channels, and have provided quantitative predictions for the evolution of channel width. Finite element modeling of the formation and propagation of cleared dislocation channels in irradiated stainless steel has provided a robust quantitative description of micro- and meso-scale localized deformation processes [101].

6. Conclusions

Steady progress has been achieved over the past several decades in developing improved high-performance steels for fossil and nuclear energy systems. The design of high-performance radiation-resistant materials can be accelerated by increased reliance on science-based multiscale models that are experimentally validated using advanced characterization tools. At the present time, modeling is being effectively used to guide the design of new high performance steels, and to gain a clear understanding of fundamental deformation mechanisms in unirradiated and irradiated steels. However, improved linkage between disparate models developed at different length and time scales is needed.

Acknowledgments

References

[1] E.E. Bloom, J. Nucl. Mater. 258-263 (1998) 7.
[2] K. Ehrlich, Philos. Trans. Roy. Soc. Lond., A 357 (1999) 595.
[3] K. Ehrlich, E.E. Bloom, T. Kondo, J. Nucl. Mater. 283-287 (2000) 79.
[4] D.L. Smith, M.C. Billone, S. Majumdar, R.F. Mattas, D.-K. Sze, J. Nucl. Mater. 258–263 (1998) 65.
[5] A.A.F. Tavassoli, J. Nucl. Mater. 302 (2002) 73.
[6] E.E. Bloom, S.J. Zinkle, F.W. Wiffen, J. Nucl. Mater. 329–333 (2004) 12.
[7] S.J. Zinkle, Fusion Eng. Des. 74 (2005) 31.

[8] E.E. Bloom et al., J. Nucl. Mater. 367–370 (2007) 1.
[9] J. Pamela, A. Becoulet, D. Borba, J.L. Boutard, L. Horton, D. Maisonnier, Fusion Eng. Des. 84 (2009) 194.
[10] B. Raj, K.B.S. Rao, J. Nucl. Mater. 386 (2009) 935.
[11] S.J. Zinkle, J.T. Busby, Mater. Today 12 (2009) 12.
[12] Y. Katoh et al., J. Nucl. Mater. 367–370 (2007) 659.
[13] L.H. Rovner, G.R. Hopkins, Nucl. Technol. 29 (1976) 274.
[14] L.L. Snead, R.H. Jones, A. Kohyama, P. Fenici, J. Nucl. Mater. 233–237 (1996) 26.
[15] R.L. Klueh, K. Ehrlich, F. Abe, J. Nucl. Mater. 191–194 (1992) 116.
[16] R.L. Klueh, A.T. Nelson, J. Nucl. Mater. 371 (2007) 37.
[17] A. Kohyama, A. Hishinuma, D.S. Gelles, R.L. Klueh, W. Dietz, K. Ehrlich, J. Nucl. Mater. 233–237 (1996) 138.
[18] A.A.F. Tavassoli et al., J. Nucl. Mater. 329-333 (2004) 257.
[19] D.T. Hoelzer, J. Bentley, M.A. Sokolov, M.K. Miller, G.R. Odette, M.J. Alinger, J. Nucl. Mater. 367–370 (2007) 166.
[20] R.L. Klueh, J.P. Shingledecker, R.W. Swindeman, D.T. Hoelzer, J. Nucl. Mater. 341 (2005) 103.
[21] R. Lindau et al., Fusion Eng. Des. 75–79 (2005) 989.
[22] G.R. Odette, M.J. Alinger, B.D. Wirth, Annu. Rev. Mater. Res. 38 (2008) 471.
[23] S. Ukai, M. Fujiwara, J. Nucl. Mater. 307–311 (2002) 749.
[24] S.J. Zinkle, Phys. Plasmas 12 (2005) 058101.
[25] H.J. Frost, M.F. Ashby, Deformation Mechanism Maps: The Plasticity and Creep of Metals and Ceramics, Pergamon Press, New York, 1982.
[26] M. Li, S.J. Zinkle, J. Nucl. Mater. 361 (2007) 192.
[27] K. Suzuki, S. Jitsukawa, N. Okubo, F. Takata, Nucl. Eng. Des. 240 (2010) 1290.
[28] D. Teirlinck, F. Zok, J.D. Embury, M.F. Ashby, Acta Metall. 36 (1988) 1213.
[29] S.J. Zinkle, G.E. Lucas, in: Fusion Materials Semiann. Progress Report for Period ending June 30, 2003, DOE/ER-0313/34, Oak Ridge National Lab, 2003. p. 101.
[30] T.S. Byun, K. Farrell, Acta Mater. 52 (2004) 1597.
[31] J. Gittus, Creep, Viscoelasticity and Creep Fracture in Solids, John Wiley & Sons, New York, 1975.
[32] P.J. Karditsas, Fusion Eng. Des. 84 (2009) 2104.
[33] M.A. Meyers, D.J. Benson, O. Vöhringer, B.K. Kad, Q. Xue, H.H. Fu, Mater. Sci. Eng. A 322 (2002) 194.
[34] G.R. Odette, T. Yamamoto, H.J. Rathbun, M.Y. He, M.L. Hribernik, J.W. Rensman, J. Nucl. Mater. 323 (2003) 313.
[35] A.A.F. Tavassoli, J. Nucl. Mater. 258–263 (1998) 85.
[36] J. Aktaa, C. Petersen, J. Nucl. Mater. 389 (2009) 432.
[37] G.-H. Koo, J.-H. Lee, Int. J. Press. Ves. Pip. 84 (2007) 284.
[38] T.S. Byun, K. Farrell, J. Nucl. Mater. 326 (2004) 86.
[39] T.S. Byun, K. Farrell, M. Li, Acta Mater. 56 (2008) 1056.
[40] G.E. Lucas, J. Nucl. Mater. 206 (1993) 287.
[41] H. Trinkaus, J. Nucl. Mater. 133–134 (1985) 105.
[42] A.V. Barashev, S.I. Golubov, Philos. Mag. 89 (2009) 2833.
[43] F.A. Garner, M.B. Toloczko, B.H. Sencer, J. Nucl. Mater. 276 (2000) 123.
[44] T. Okita, W.G. Wolfer, J. Nucl. Mater. 327 (2004) 130.
[45] S.J. Zinkle, N.M. Ghoniem, Fusion Eng. Des. 51–52 (2000) 55.
[46] N.M. Ghoniem, R.W. Conn, in: Fusion Reactor Design and Tech., II, IAEA-TC-392/62, International Atomic Energy Agency, Vienna, 1983, p. 389.
[47] G.E. Lucas, G.R. Odette, Nuclear Engineering and Design/Fusion 2 (1985) 145.
[48] S. Majumdar, G. Kalinin, J. Nucl. Mater. 283–287 (2000) 1424.
[49] R.L. Klueh, Int. Mater. Rev. 50 (2005) 287.
[50] R. Viswanathan, Adv. Mater. Process. 162 (2004) 73.
[51] S.J. Piet, E.T. Cheng, S. Fetter, J.S. Herring, Fusion Technol. 19 (1991) 146.
[52] D.S. Gelles, M.L. Hamilton, J. Nucl. Mater. 148 (1987) 272.
[53] J.L. Boutard, A. Alamo, R. Lindau, M. Rieth, Comptes Rend. Phys. 9 (2008) 287.
[54] R.L. Klueh, D.R. Harries, High-chromium ferritic and martensitic steels for nuclear applications, American Society for Testing and Materials, West Conshohocken, PA, 2001.
[55] N.M. Ghoniem, A. Shabaik, M.Z. Youssef, in: J.W. Davis, D.J. Michel (Eds.), Topical Conf. On Ferritic Alloys for Use in Nuclear Energy Technologies, Snowbird, Utah, TMS-AIME, Warrendale, PA, 1983, p. 201.
[56] E.E. Bloom et al., J. Nucl. Mater. 122–123 (1984) 17.
[57] D.R. Harries, G.J. Butterworth, A. Hishinuma, F.W. Wiffen, J. Nucl. Mater. 191–194 (1992) 92.
[58] A. Hishinuma, A. Kohyama, R.L. Klueh, D.S. Gelles, W. Dietz, K. Ehrlich, J. Nucl. Mater. 258–263 (1998) 193.
[59] S. Jitsukawa et al., J. Nucl. Mater. 329–333 (2004) 39.
[60] R.L. Klueh, Curr. Opin. Sol. State Mater. Sci. 8 (2004) 239.
[61] B. van der Schaaf et al., Fusion Eng. Des. 69 (2003) 197.
[62] G.B. Olson, Science 277 (1997) 1237.
[63] J.M. Vitek, M.L. Santella, ORNL (2010).
[64] P.J. Maziasz, J.P. Shingledecker, N.D. Evans, M. Pollard, J. Press. Ves. Technol.-Trans. ASME 131 (2009) 051404.
[65] M.P. Brady, Y. Yamamoto, M.L. Santella, L.R. Walker, Oxid. Metals 72 (2009) 311.
[66] Y. Yamamoto et al., Science 316 (2007) 433.
[67] Y. Yamamoto, M.L. Santella, M.P. Brady, Metall. Mater. Trans. A 40A (2009) 1868.
[68] F. Abe, Mater. Sci. Eng. A 510–511 (2009) 64.
[69] M. Taneike, F. Abe, K. Sawada, Nature 424 (2003) 294.
[70] A.A. Barani, F. Li, P. Romano, D. Ponge, D. Raabe, Mater. Sci. Eng. A 463 (2007) 138.
[71] S. Hollner et al., J. Nucl. Mater. 405 (2010) 101.
[72] R.L. Klueh, N. Hashimoto, P.J. Maziasz, Scripta Mater. 53 (2005) 275.
[73] R.L. Klueh, N. Hashimoto, P.J. Maziasz, J. Nucl. Mater. 367–370 (2007) 48.
[74] D. Raabe, D. Ponge, O. Dmitrieva, B. Sander, Adv. Eng. Mater. 11 (2009) 547.
[75] D.A. McClintock, M.A. Sokolov, D.T. Hoelzer, R.K. Nanstad, J. Nucl. Mater. 392 (2009) 353.
[76] R.J. Kurtz et al., J. Nucl. Mater. 386–388 (2009) 411.
[77] J. Isselin, R. Kasada, A. Kimura, Corros. Sci. 52 (2010) 3266.
[78] H.S. Cho, A. Kimura, S. Ukai, M. Fujiwara, J. Nucl. Mater. 329–333 (2004) 387.
[79] S. Takaya et al., J. Nucl. Mater. 386–388 (2009) 507.
[80] M.J. Alinger, G.R. Odette, D.T. Hoelzer, Acta Mater. 57 (2009) 392.
[81] Z. Oksiuta, P. Olier, Y. De Carlan, N. Baluc, J. Nucl. Mater. 393 (2009) 114.
[82] S. Hao, W.K. Liu, B. Moran, F. Vernerey, G.B. Olson, Comp. Meth. Appl. Mech. Eng. 193 (2004) 1865.
[83] S. Hao, B. Moran, W.K. Liu, G.B. Olson, J. Comp.-Aided Mater. Des. 10 (2003) 99.
[84] E. Pink, R.J. Arsenault, Prog. Mater. Sci. 24 (1979) 1.
[85] N. Choly, G. Lu, E. Weinan, E. Kaxiras, Phys. Rev. B 71 (2005) 094101.
[86] C. Woodward, S.I. Rao, Phys. Rev. Lett. 88 (2002) 216402.
[87] D.R. Trinkle, C. Woodward, Science 310 (2005) 1665.
[88] G. Lu, E.B. Tadmor, E. Kaxiras, Phys. Rev. B 73 (2006) 024108.
[89] Z.Z. Chen, G. Lu, N. Kioussis, N.M. Ghoniem, Phys. Rev. B 78 (2008) 134102.
[90] N. Kioussis, N.M. Ghoniem, J. Computat. Theor. Nanosci. 7 (2010) 1317.
[91] G.F. Wang, A. Strachan, T. Cagin, W.A. Goddard, Phys. Rev. B 68 (2003) 224101.
[92] M.S. Duesbury, V. Vitek, Acta Mater. 46 (1998) 1481.
[93] S. Lozano-Perez, M.L. Jenkins, J.M. Titchmarsh, Philos. Mag. Lett. 86 (2006) 367.
[94] W.J. Phythian, C.A. English, J. Nucl. Mater. 205 (1993) 162.
[95] D.J. Bacon, Y.N. Osetsky, Philos. Mag. 89 (2009) 3333.
[96] Z.Z. Chen, N. Kioussis, N.M. Ghoniem, Phys. Rev. B 80 (2009) 184104.
[97] A. Takahashi, N.M. Ghoniem, J. Mech. Phys. Solids 56 (2008) 1534.
[98] A. Takahashi, Z. Chen, N. Kioussis, N.M. Ghoniem, in: ICFRM-14, these proceedings, 2009.
[99] D.M. Dimiduk, C. Woodward, R. LeSar, M.D. Uchic, Science 312 (2006) 1188.
[100] N. Hashimoto, S.J. Zinkle, A.F. Rowcliffe, J.P. Robertson, S. Jitsukawa, J. Nucl. Mater. 283–287 (2000) 528.
[101] M. Sauzy, K. Bavard, W. Karlsen, J. Nucl. Mater. 406 (2010) 152.
[102] H.-J. Lee, B.D. Wirth, Philos. Mag. 89 (2009) 821.
[103] J. Marian, E. Martinez, H.-J. Lee, B.D. Wirth, J. Mater. Res. 24 (2009) 3628.
[104] Y.N. Osetsky, D. Rodney, D.J. Bacon, Philos. Mag. 86 (2006) 2295.
[105] G. Monnet, Y.N. Osetsky, D.J. Bacon, Philos. Mag. 90 (2010) 1001.
[106] D. Rodney, Nucl. Instrum. Methods Phys. Res. B 228 (2005) 100.
[107] Y. Matsukawa, Y.N. Osetsky, R.E. Stoller, S.J. Zinkle, Philos. Mag. 88 (2008) 581.
[108] T.S. Byun, K. Farrell, M. Li, Acta Mater. 56 (2008) 1044.
[109] N.M. Ghoniem, E.P. Busso, N. Kioussis, H.C. Huang, Philos. Mag. 83 (2003) 3475.
[110] R.J. Amodeo, N.M. Ghoniem, Phys. Rev. B 41 (1990) 6958.
[111] J. Lepinoux, L.P. Kubin, Scripta Metall. 21 (1987) 833.
[112] T. Nogaret, D. Rodney, M. Fivel, C. Robertson, J. Nucl. Mater. 380 (2008) 22.